Hamiltonian Dynamics of Protein Filament Formation

Thomas C. T. Michaels, Samuel I. A. Cohen, Michele Vendruscolo, Christopher M. Dobson, and Tuomas P. J. Knowles[*]

Department of Chemistry, University of Cambridge, Lensfield Road, Cambridge CB2 1EW, United Kingdom

We establish the Hamiltonian structure of the rate equations describing the formation of protein filaments. We then show that this formalism provides a unified view of the behavior of a range of biological self-assembling systems as diverse as actin, prions, and amyloidogenic polypeptides. We further demonstrate that the time-translation symmetry of the resulting Hamiltonian leads to previously unsuggested conservation laws that connect the number and mass concentrations of fibrils and allow linear growth phenomena to be equated with autocatalytic growth processes. We finally show how these results reveal simple rate laws that provide the basis for interpreting experimental data in terms of specific mechanisms controlling the proliferation of fibrils.

The formation of protein filaments is associated with a wide range of cellular functions, including transport and scaffolding [1,2], as well as a variety of human disorders, such as Alzheimer's, Parkinson's and prion diseases [3,4]. The formal description of protein filament growth kinetics was initiated by Oosawa [1,2] for polymer systems growing through primary nucleation and filament elongation and was later generalized [5–7] to include secondary pathways, where existing aggregates multiply in number, e.g., through fragmentation [8–10], lateral branching [6,11,12], or surface-catalyzed nucleation [7,13,14]. The general mathematical approach underlying these descriptions considers mean-field master equations for the lowest moments of the filament length distribution, which correspond to the most commonly accessible experimental measurements of the total number and mass of filaments [1,2,7,15,16]

$$\frac{dm(t)}{dt} = -2k_+ m(t)P(t), \qquad (1)$$

$$\frac{dP(t)}{dt} = k_n m(t)^{n_c} + k_2 m(t)^{n_2}[m_{\text{tot}} - m(t)], \qquad (2)$$

where $m(t)$ is the concentration of soluble monomer, $P(t)$ is the number concentration of aggregates, m_{tot} is the total mass of proteins and $M(t) = m_{\text{tot}} - m(t)$ is the filament mass. Equation (1) describes the consumption of monomers through their incorporation onto the ends of existing filaments, with the rate constant describing elongation given by k_+. The rate constants k_n and k_2 are those of the primary and secondary nucleation, respectively, and the terms in Eq. (2) describe the formation of new aggregates via these pathways with the exponents n_c and n_2 defining the dependencies of these processes on the free monomer concentration: $n_2 = 0$ corresponds to filament fragmentation [8,9,15], $n_2 = 1$ pertains to a secondary process with a linear dependence on the monomer concentration, an

example of which is lateral branching [6,11,12], whereas higher exponents $n_2 \geq 2$ arise in the presence of heterogeneous nucleation where the surfaces of filaments catalyze the nucleation of new aggregates from monomers [7,13,14].

The defining equations (1) and (2) are coupled nonlinear equations that have been described for the past three decades as not readily integrable [6,7]. New insights into the behavior of the system have recently emerged from an analysis that utilizes fixed-point theory to generate self-consistent solutions to the rate laws [15,18], but the complexity of the self-assembly process has continued to preclude the development of a general theoretical framework to account quantitatively for the kinetics in all cases. Here, we show that it is possible to achieve this goal by establishing the Hamiltonian structure of this classical equation system [19].

By analogy with classical mechanics, we define a momentum coordinate as $p(t) = 2k_+ P(t)$ and a position coordinate $q(t) = \log[m_{\text{tot}}/m(t)]$, which emerges naturally by imposing $p = \dot{q}$ in Eq. (1). This identification allows Eqs. (1) and (2) to be cast into canonical form $\dot{q} = \partial\mathcal{H}/\partial p$, $\dot{p} = -\partial\mathcal{H}/\partial q$. The resulting Hamiltonian takes the form $\mathcal{H} = p^2/2 + V(q)$, with potential function

$$V(q) = \lambda^2 \frac{e^{-n_c q}}{n_c} + \kappa^2 \frac{e^{-n_2 q}[(n_2+1) - n_2 e^{-q}]}{n_2(n_2+1)}, \qquad (3)$$

where $\lambda = \sqrt{2k_+ k_n m_{\text{tot}}^{n_c}}$ and $\kappa = \sqrt{2k_+ k_2 m_{\text{tot}}^{n_2+1}}$ are effective rate constants for proliferation driven by primary nucleation [1,2] and secondary nucleation [7,15,28], respectively. This Hamiltonian admits an interesting mechanical analogy. The position coordinate q measures the increase of fibril mass during filament growth. The momentum p is proportional to the number of filament ends, and the kinetic energy term $p^2/2$ depends on the square of the momentum. So at twice the number of ends, the system has twice the momentum and four times the

energy of motion. This kinetic energy term measures the propensity of the system to move in position coordinate q, i.e., to consume monomer subunits and form aggregates. In the next two sections, we associate the potential energy term $V(q)$ with the driving force for filamentous growth (see Fig. 1).

Conservation of energy.—The nonlinear and coupled nature of the moment equations (1) and (2) has made them challenging to study [6,7], leading to a range of specialized numerical and analytical approaches. Here, the reduction to canonical form allows us, instead, to follow the same general program as in classical mechanics. The total energy of the linearly assembling system is the sum of its kinetic and potential energy terms, whereby the potential energy decomposes into single contributions from each of the active nucleation pathways [29]. Because the Hamiltonian is time translationally invariant, $\partial \mathcal{H}/\partial t = 0$, the total energy of the system is conserved: $\mathcal{H} = V(0) = \lambda^2/n_c + \kappa^2\theta^2/2$, where $\theta = \sqrt{2/[n_2(n_2+1)]}$; by consequence, the generation of new filaments growth ends through nucleation can be interpreted as the conversion of potential energy into kinetic energy [30]. The system, therefore, moves along the orbits $\mathcal{H}(p,q) = V(0)$, revealing a simple relationship between the number and the mass of fibrils: $p(t) = \sqrt{2[V(0) - V(q)]}$ corresponding to the fact that, in a linearly assembling system, aggregates grow in such a way that their total number and mass obey the energy conservation relationship at all times.

Euler-Lagrange equation.—The next step in our program involves introducing the Lagrangian $\mathcal{L} = \dot{q}^2/2 - V(q)$ by exchanging p for $\dot{q} = p$, which leads to the Euler-Lagrange (EL) equation $\ddot{q} = -\partial_q V$. Within the classical mechanical analogy, the term $-\partial_q V$ is interpreted, therefore, as the driving force of the assembly reaction, whose form is defined by the specific dependence of the various nucleation mechanisms on the concentrations of monomers and aggregates (Fig. 1), leading, in the case of secondary nucleation, to a nonmonotonic driving force. Interestingly, the potential function, Eq. (3), reveals that the time evolution of $q(t)$, as described by the EL equation, depends on combinations of the rate constants, $k_+ k_n$ or $k_+ k_2$, via the

FIG. 1. Potential energy terms and associated driving forces for primary nucleation and secondary processes.

parameters λ and κ for each active nucleation mechanism. This conclusion is consistent with the observation that if a specific primary or secondary mechanism is dominant, then the reaction kinetics are dominated by the corresponding combined rate parameter [1,13,15,18].

Scaling behaviors.—Integrating the EL equation once, or equivalently combining the conservation of energy relationship with the identification $\dot{q} = p$, provides an implicit solution for $q(t)$ in terms of a single integral

$$t = \int_0^q \frac{dq'}{\sqrt{2[V(0) - V(q')]}}. \tag{4}$$

Equation (4) provides additional insights into the scaling behavior of the system. The key phenomenological observable considered in the literature is the time τ at which a certain fraction of the monomer has been consumed [e.g., the half-time where $q(\tau) = \log 2$]. When the rate of the secondary process vanishes, $V(0) - V(q) \sim \lambda^2$; thus, Eq. (4) recovers the scaling law $\tau \sim \lambda^{-1} \sim m_{\text{tot}}^{-n_c/2}$ derived in the Oosawa theory [i.e., Eqs. (1) and (2) with $k_2 = 0$] [1,2]. In the opposite limit, where the secondary pathway dominates, Eq. (4) indicates a transition to an inverse scaling of the half-time with κ such that $\tau \sim \kappa^{-1} \sim m_{\text{tot}}^{-(n_2+1)/2}$ (see the Supplemental Material [21]). It is interesting to note, therefore, that the total energy of the system is closely related to the sum of the relevant system time scales.

Integrated rate laws.—Integrated rate laws provide a convenient means of establishing the values of the microscopic rates for each step in the assembly pathway from experimental measurements. Equation (4) makes it possible to investigate the existence of such integrated rate laws for filamentous growth processes. Previously, it has been assumed in the literature that Eqs. (1) and (2) have no exact closed form solutions in terms of elementary functions when secondary pathways are active. Interestingly, however, the reduction of the problem to quadrature, Eq. (4), shows that for $n_2 = 1$ and $n_c = 1$ or $n_c = 2$, Eqs. (1) and (2) admit an exact solution

$$e^{-q(t)} = \frac{m(t)}{m_{\text{tot}}} = \frac{\nu^2}{\lambda^2 \cosh(\nu t) + \nu^2 - \lambda^2}, \tag{5}$$

where $\nu = \sqrt{\kappa^2 + 2\lambda^2}$ for $n_c = 1$ and $\nu = \sqrt{\kappa^2 + \lambda^2}$ for $n_c = 2$. Equation (5) is, to our knowledge, the first exact, mass-conserving solution to be presented for filamentous growth with secondary pathways. Strikingly, the effective proliferation rate ν that emerges from Eq. (5) interpolates between the combined rate constants for growth through by primary, λ, and secondary, κ, pathways.

Sigmoidal-type kinetics result from many different microscopic processes, perhaps the best known being the case of simple autocatalytic processes, $A + B \rightarrow 2B$. Because of the similarity in overall shape, logistic and other similar functions are commonly used to analyze
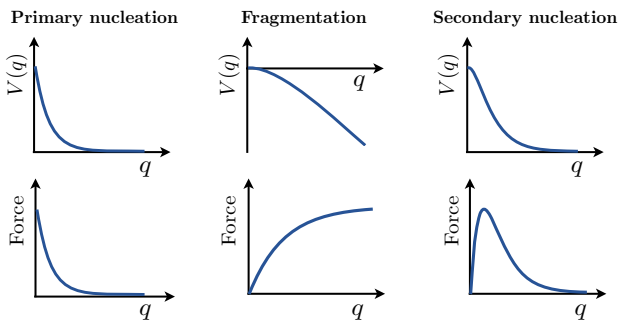
filament growth kinetics. Equation (5) clearly shows that
these types of functions do, indeed, emerge from the rate
laws [31]. Unlike in the case of classical autocatalytic
growth, however, the parameter ν in Eq. (5) does not relate
to an individual microscopic rate constant, but rather
corresponds to a complex combination of the rate constants
and the monomer concentration.

System behavior when secondary processes dominate.—
Although the reduction to quadrature makes it possible to
directly connect the case $n_2 = 1$ to classical autocatalytic
growth, for higher values of the nucleation exponents,
Eq. (4) involves elliptic integrals which neither reduce to
elementary functions nor can be inverted to yield $q(t)$ in
closed form. Despite the nonexistence of exact closed form
solutions beyond the case $n_2 = 1$, a more general relation-
ship to autocatalytic descriptions does in fact exist when the
reaction kinetics are dominated by the secondary mecha-
nism, which is defined by the condition $\kappa \gg \lambda$. To motivate
this connection, note that, in the case $n_2 = 1$, neglecting the
term proportional to λ in the potential energy Eq. (3) leads
to the simplified energy conservation relationship
$p(t) = \kappa(1 - e^{-q})$. This proportionality between the poly-
mer number and monomer concentrations emerges because
the rate at which monomers are incorporated into fibrils
through elongation and the rate at which fibrils are created
through the secondary process are both linear in the
monomer concentration. When substituted into Eq. (1),
this linear energy relationship yields the well-known
logistic differential equation [31].

The simplified form of the energy relationship noted above
can be generalized to any secondary nucleation exponent
by considering the behavior of the system at early and late
times. In particular, linearization of the moment Eqs. (1) and
(2) shows that the polymer number and monomer concen-
trations initially grow exponentially with the same exponent
[6,7], κ, independently of the value of n_2; by fixing the late
time limit $P(\infty) = \theta\kappa/(2k_+)$, which emerges from the
Hamiltonian $\mathcal{H}(0) = \mathcal{H}(\infty) = p(\infty)^2/2$ at long times, it
is then possible to construct (see the Supplemental Material
[21]) a simplified energy conservation relationship that is
valid and accurate for all values of n_2 [32]

$$\frac{P(t)}{P(\infty)} = 1 - e^{-q(t)/\theta} = 1 - \left(\frac{m(t)}{m_{\text{tot}}}\right)^{(1/\theta)}. \qquad (6)$$

Interestingly, a similar energy relationship holds when only
primary nucleation pathways are active, $P(t)/P(\infty) =
\sqrt{1 - e^{-n_c q}}$, where the square-root can be rationalized since
for early times $P \sim t$, $M \sim t^2$ [2,18]. Application of the
generalized energy relationship Eq. (6) into Eq. (1) results in
the generalized logistic (Richards) differential equation,
yielding the solution

$$e^{-q(t)} = \frac{m(t)}{m_{\text{tot}}} = \left[1 + \frac{\lambda^2}{2\kappa^2\theta}e^{\kappa t}\right]^{-\theta}. \qquad (7)$$

Note that, because the derivation of Eq. (7) neglects
primary nucleation, a critical concentration of filaments
$M \sim m_{\text{tot}}\lambda^2/(2\kappa^2)$ has been introduced in the integration
to seed the system so that the resulting expression for $m(t)$
matches the leading order term for early times [15,18]. This
critical concentration corresponds to the point at which the
potential term in Eq. (3) driven by the secondary process
becomes larger than the term relating to primary nucleation.
We also note that in the case $n_2 = 1$, corresponding to $\theta = 1$,
Eq. (7) recovers the logistic function. Moreover, in the
special case $n_2 = 0$, corresponding to breakable filaments,
Eq. (7) reduces to a Gompertz autocatalytic function [33]
$m(t)/m_{\text{tot}} = \exp[-\lambda^2 e^{\kappa t}/(2\kappa^2)]$ as demonstrated by exploit-
ing the identity $\lim_{b\to\infty}(1 + a/b)^b = e^a$, with the energy
conservation equation Eq. (6) reducing to $P(t) = \kappa q(t)/
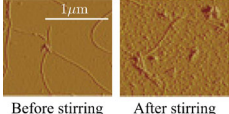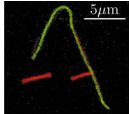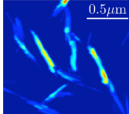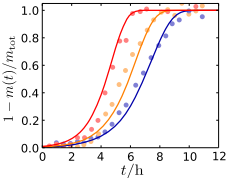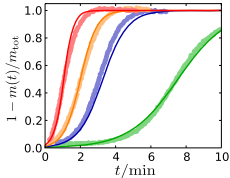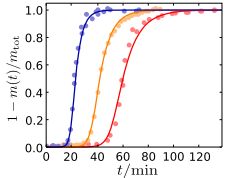(2k_+) = \kappa/(2k_+) \log[m_{\text{tot}}/m(t)]$.

Equation (7) gives, in closed form, the time evolution of
the monomer concentration in a system dominated by a
secondary nucleation pathway. This result shows that
different autocatalytic descriptions are required to capture
the characteristic shapes of the reaction profiles and the
scaling behavior that is associated with the actions of the
different secondary pathways. While variations of logistic
functions have been used to fit protein aggregation data
[34,35], the specific form derived here, Eq. (7), is different
from the forms commonly used.

Unified analysis of experimental data.—Using the sim-
ple integrated rate laws that have emerged, we now show
that mechanistic information and the microscopic rate
constants can be extracted, using a global analysis [36],
from a range of experimental data describing protein
aggregation in diverse systems ranging from functional
to disease-associated systems, as shown in Table I.

The aggregation of the yeast prion Ure2p involves
filament fragmentation [9,39], and the data are, therefore,
fitted to a Gompertz function ($n_2 = 0$). The Arp 2/3
complex, when activated by Wiskott–Aldrich Syndrome
protein (WASP), has been observed to initiate branch points
along the sides of actin filaments [12,40] ($n_2 = 1$); the data
for actin can, therefore, be fitted to the logistic form.
Finally, the self-assembly of the islet amyloid polypeptide
(IAPP) involves a nucleation step ($n_2 = 4$) that is catalyzed
by the surfaces of existing filaments [13], and is, therefore,
described by Eq. (7) with $\theta = 1/\sqrt{10}$. For each system, the
data are fitted with two global fitting parameters corre-
sponding to the combinations of the microscopic rate
parameters from λ and κ in Eq. (7).

The integrated rate laws for the three secondary mech-
anisms in Table I correspond to variations of autocatalytic
growth, which is a consequence of the different depend-
encies of the secondary nucleation processes on the free
monomer concentration. All three systems show an
exponential initial phase. The data for actin, controlled
by lateral growth, is approximately symmetric about the
time to half-completion. In contrast, the data pertaining to

TABLE I.   Connection between filamentous growth dominated by a secondary pathway and autocatalytic processes [33]. The data for the yeast prion (Ure2p) are from Ref. [37]; the data for actin are from Ref. [38] and have $n_c = 3$ [1,2]; the data for IAPP are from Ref. [13] and have $n_2 = 4$ [13], $n_c = 8$. The reaction profiles shown for each protein system correspond to reactions beginning from increasing initial concentrations of monomer: m_{tot}: 20 μM [blue], 25 μM [orange], 38 μM [red] (yeast prion); 2 μM [green], 4 μM [blue], 6 μM [orange], 10 μM [red] (actin); 700 μM [blue], 800 μM [orange], 1000 μM [red] (IAPP). The data sets are each fitted with the two microscopic global parameters, k_+k_2 and k_n/k_2, that appear in the phenomenological parameter identifications for a, b. The images are from Refs. [12,39], and [13]. Fit parameters: $k_+k_2 = 9.8 \times 10^{-4}$ M^{-1} s^{-2}, $k_n/k_2 = 10^3$ M^{-1} (yeast prion); $k_+k_2 = 1.8 \times 10^7$ M^{-2} s^{-2}, $k_n/k_2 = 4.4 \times 10^3$ M^{-1} (actin); $k_+k_2 = 6.4 \times 10^{10}$ M^{-5} s^{-2}, $k_n/k_2 = 960$ M^{-3} (IAPP).

	Yeast prion (Ure2p)	Actin (with Arp 2/3 + WASp)	Amyloidogenic peptide (IAPP)
Example system	Before stirring After stirring		
Secondary nucleation exponent	$n_2 = 0$	$n_2 = 1$	$n_2 \geq 2$
Corresponding mechanism	Fragmentation	Lateral branching	Surface nucleation
Analogous system	Gompertz	Logistic	Richards
Integrated rate law $m(t)/m_{\text{tot}} \approx$	$\exp(-ae^{bt})$	$1/(1 + ae^{bt})$	$1/[1 + ae^{bt}/c]^c$
Microscopic parameter identification	$a = k_n m_{\text{tot}}^{n_c-n_2-1}/[2k_2]$	$b = \sqrt{2k_+k_2 m_{\text{tot}}^{n_2+1}}$	$c = \sqrt{2/[n_2(n_2+1)]}$
Global fit to data			
Asymmetry about the time to half-completion	Sharper approach to plateau relative to early stage growth	Approximately symmetric	Less sharp approach to plateau relative to early stage growth

fragmentation and surface-catalysis dominated systems show opposite asymmetries about the half-time, with the aggregation of the yeast prion slowing down towards the end of the reaction more rapidly than the acceleration at the beginning of the reaction, and IAPP showing the opposite asymmetry. These characteristic (a)symmetries are the difference between Gompertz ($n_2 = 0$), logistic ($n_2 = 1$), and Richards ($n_2 \geq 2$) autocatalytic behavior, and demonstrate the need to use chemical kinetic analysis in order to establish the correct functional form to describe a given mechanism.

It is also important to note that fitting even the correct functional form in an empirical manner does not reveal the relationship between the fitting parameters and the true microscopic rate constants, Table I. Moreover, without knowledge of how the phenomenological parameters in a fitting function depend on the monomer concentration, a global analysis is not possible and the scaling behavior with respect to the monomer concentration is not recovered (see the Supplemental Material [21]).

Finally, from the analysis of the kinetic data, we can also directly test the predictions that have emerged from energy conservation for filamentous growth processes. Figures 2(a)–2(c) show experimental data for the three systems in Table I and the predicted relationships between

the polymer number and monomer concentrations that have emerged as a consequence of conservation of energy, Eq. (6). Moreover, overlaying all of the experimental data and plotting, in Fig. 2(d), the Hamiltonian from Eq. (3) as a function of time verifies that $\mathcal{H}(t) = \mathcal{H}(0)$ is, indeed, conserved in filamentous growth processes.

Summary and outlook.—Despite extensive study in the literature over the past five decades, many advances in the study of filamentous growth have been system dependent, suggesting that each filament system requires a unique suite of analytical and numerical tools to understand its behavior. Here, by showing that the fundamental equations describing filament formation possess canonical Hamiltonian structure, we have, instead, been able to apply the general tools of classical mechanics to provide a unified theoretical framework for understanding the behavior of this system. Using this approach, we have derived previously unsuggested connections between the polymer number and monomer concentrations and have established simple closed form solutions that can be used to analyze experimental measurements. Looking forward, with the increasing availability of quantitative data, this approach could move us closer to the construction of a general dynamical theory of self-assembly processes, which represent some of the most fundamental and inspiring aspects of biological systems.
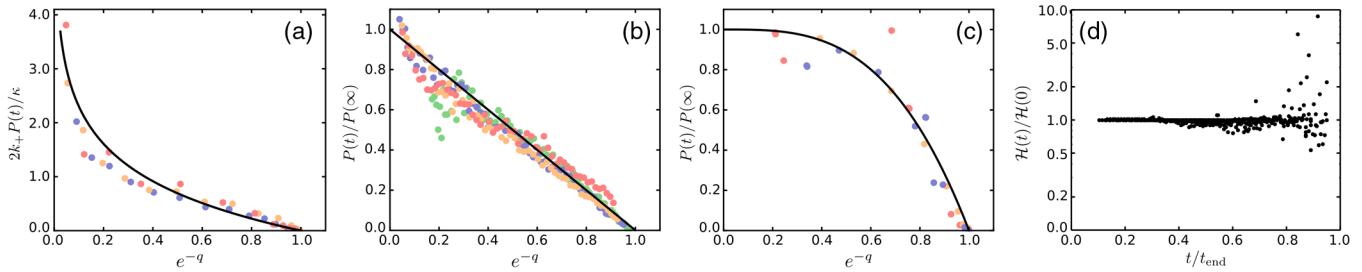
FIG. 2.   Conservation relationships for filament systems growing through various secondary pathways. The systems, data sources, and color coding are the same as in Table I: (a) yeast prion (Ure2p); (b) actin (with Arp 2/3 + WASP); (c) IAPP. The solid lines in (a)–(c) show the predicted energy relationships between the polymer number (see the Supplemental Material [21]) and monomer concentrations that emerge from energy conservation: (a) $2k_+ P(t)/\kappa = q(t) = -\log[m(t)/m_{tot}]$; (b), (c) $P(t)/P(\infty) = 1 - e^{-q(t)/\theta} = 1 - [m(t)/m(0)]^{1/\theta}$ with $\theta = 1$ (b) or $\theta = 1/\sqrt{10}$ (c). (d) shows the Hamiltonian from Eq. (3) overlaid for all of the data, verifying that $\mathcal{H}(t) = \mathcal{H}(0)$ is conserved. Data in (a)–(c) are plotted as a function of $e^{-q(t)} = m(t)/m_{tot}$. The time values in (d) are normalized by the time, t_{end}, at which $1 - m(t)/m_{tot}$ reaches a plateau. The scatter in the data for later times in (d) is due to increased experimental noise for $P(t)$ as the reaction profiles reach a plateau.

*tpjk2@cam.ac.uk

[1] F. Oosawa and M. Kasai, J. Mol. Biol. **4**, 10 (1962).
[2] F. Oosawa, and S. Asakura, *Thermodynamics of the Polymerization of Protein* (Academic Press, New York, 1975).
[3] C. M. Dobson, Nature (London) **426**, 884 (2003).
[4] F. Chiti and C. M. Dobson, Annu. Rev. Biochem. **75**, 333 (2006).
[5] F. A. Ferrone, J. Hofrichter, H. R. Sunshine, and W. A. Eaton, Biophys. J. **32**, 361 (1980).
[6] M. F. Bishop and F. A. Ferrone, Biophys. J. **46**, 631 (1984).
[7] F. A. Ferrone, J. Hofrichter, and W. A. Eaton, J. Mol. Biol. **183**, 611 (1985).
[8] A. Wegner and P. Savko, Biochemistry **21**, 1909 (1982).
[9] S. R. Collins, A. Douglass, R. D. Vale, and J. S. Weissman, PLoS Biol. **2**, e321 (2004).
[10] W.-F. Xue, S. W. Homans, and S. E. Radford, Proc. Natl. Acad. Sci. U.S.A. **105**, 8926 (2008).
[11] C. B. Andersen, H. Yagi, M. Manno, V. Martorana, T. Ban, G. Christiansen, D. E. Otzen, Y. Goto, and C. Rischel, Biophys. J. **96**, 1529 (2009).
[12] K. J. Amann and T. D. Pollard, Nat. Cell Biol. **3**, 306 (2001).
[13] A. M. Ruschak and A. D. Miranker, Proc. Natl. Acad. Sci. U.S.A. **104**, 12341 (2007).
[14] A. Cacciuto, S. Auer, and D. Frenkel, Nature (London) **428**, 404 (2004).
[15] T. P. J. Knowles, C. A. Waudby, G. L. Devlin, S. I. A. Cohen, A. Aguzzi, M. Vendruscolo, E. M. Terentjev, M. E. Welland, and C. M. Dobson, Science **326**, 1533 (2009).
[16] Note that the moment equations neglect additional terms describing the contribution of nucleation and fragmentation processes on the concentration of monomers. Although these terms are critical in determining the steady state of the

system, they do not contribute significantly to the time course of the aggregate mass concentration [2,6,17].
[17] S. I. A. Cohen, M. Vendruscolo, C. M. Dobson, and T. P. J. Knowles, J. Chem. Phys. **135**, 065107 (2011).
[18] S. I. A. Cohen, M. Vendruscolo, M. E. Welland, C. M. Dobson, E. M. Terentjev, and T. P. J. Knowles, J. Chem. Phys. **135**, 065105 (2011).
[19] Note that the framework described here can be generalized to include additional processes, such as monomer dissociation or fibril annealing [20] (see the Supplemental Material [21]).
[20] T. C. T. Michaels and T. P. J. Knowles, J. Chem. Phys. **140**, 214904 (2014).
[21] See Supplemental Material at http://link.aps.org/supplemental/10.1103/PhysRevLett.116.038101, which contains Refs. [22–27], for further discussion of the scaling behaviors, a detailed derivation and numerical validation of Eq. (6), and additional details of the fitting.
[22] M. Abramowitz and I. A. Stegun, *Handbook of Mathematical Functions with Formulas, Graphs, and Mathematical Tables* (Dover, New York, 1965).
[23] A. Vitalis and R. V. Pappu, Biophys. Chem. **159**, 14 (2011).
[24] S. Chen, F. A. Ferrone, and R. Wetzel, Proc. Natl. Acad. Sci. U.S.A. **99**, 11884 (2002).
[25] R. F. Goldstein and L. Stryer, Biophys. J. **50**, 583 (1986).
[26] F. Ferrone, Methods Enzymol. **309**, 256 (1999).
[27] S. I. A. Cohen, M. Vendruscolo, C. M. Dobson, and T. P. J. Knowles, J. Mol. Biol. **421**, 160 (2012).
[28] S. I. A. Cohen, M. Vendruscolo, C. M. Dobson, and T. P. J. Knowles, J. Chem. Phys. **135**, 065106 (2011).
[29] The sign of the potential is such that free monomers have higher potential energy than monomers in aggregates. The potential term for fragmentation is, hence, negative.
[30] We consider the case where all of the protein is initially monomeric, $q(0) = 0$; reactions with preformed fibrils can be studied using the appropriate initial conditions.
[31] The exact solution Eq. (5) is of logistic form beyond early times when $\cosh(\nu t) \sim e^{\nu t}$.
[32] The simplified energy relationship, Eq. (7), is equivalent to making the accurate approximation $1 + e^{-n_2 q}[n_2 e^{-q} - (n_2 + 1)] \approx (1 - e^{-q/\theta})^2$ in the potential Eq. (4) [21].
[33] A. Tsoularis and J. Wallace, Math. Biosci. **179**, 21 (2002).

[34] A. M. Morris, M. A. Watzky, J. N. Agar, and R. G. Finke, Biochemistry **47**, 2413 (2008).

[35] A. M. Morris, M. A. Watzky, and R. G. Finke, Biochim. Biophys. Acta **1794**, 375 (2009).

[36] In a global fit, all reaction profiles are fitted simultaneously using the same choice of values for the kinetic parameters, with the initial protein concentrations entering the integrated rate law fixed at the experimentally determined value for each reaction profile.

[37] L. Zhu, X.-J. Zhang, L.-Y. Wang, J.-M. Zhou, and S. Perrett, J. Mol. Biol. **328**, 235 (2003).

[38] H. N. Higgs, L. Blanchoin, and T. D. Pollard, Biochemistry **38**, 15212 (1999).

[39] M. Tanaka, S. R. Collins, B. H. Toyama, and J. S. Weissman, Nature (London) **442**, 585 (2006).

[40] K. J. Amann and T. D. Pollard, Proc. Natl. Acad. Sci. U.S.A. **98**, 15009 (2001).